ARTICLES

Absorption Spectrum and Cross Sections of the Allyl Radical Measured Using Cavity Ring-Down Spectroscopy: The $\tilde{A} \leftarrow \tilde{X}$ Band

Kenichi Tonokura* and Mitsuo Koshi

Department of Chemical System Engineering, Graduate School of Engineering, The University of Tokyo, 7-3-1 Hongo, Bunkyo-ku, Tokyo 113-8656, Japan

Received: March 27, 2000; In Final Form: June 15, 2000

Cavity ring-down spectroscopy (CRDS) was used to measure the electronic absorption spectrum of the allyl radical (CH_2CHCH_2) between 370 and 420 nm at 297 K. The allyl radical was produced from the 193 nm excimer laser photolysis of allylic precursors. Optimized geometries in the ground ($\tilde{X}$) and first excited ($\tilde{A}$) states and adiabatic and vertical excitation energies in the $\tilde{A} \leftarrow \tilde{X}$ transition were calculated by ab initio molecular orbital calculations at CASSCF level of theory. The equilibrium structure of the $\tilde{A}$ state was found in a nonplanar C_2 geometry with CH_2 twisted groups. The removal rate of the allyl radical associated with self-reactions by its absorption in the $\tilde{A} \leftarrow \tilde{X}$ transition was probed by CRDS. The absorption cross section of the allyl radical at 402.9 nm was determined to be $(2.0 \pm 0.4) \times 10^{-19}$ cm^2 molecule^{-1} through analysis of time-dependent absorption traces.

1. Introduction

Allyl radical (CH_2CHCH_2) is the simplest π-conjugated hydrocarbon radical having an open-shell electronic structure due to its unpaired electron. The ground state of the allyl radical has the Hartree−Fock configuration $(\text{core})(6a_1)^2(4b_2)^2(1b_1)^2(1a_2)^1$ $\tilde{X}$ $^2A_2$. The allyl radical plays a key role in high-temperature hydrocarbon combustion systems where it is involved in formation of polyacethylenes, possibly of polycyclic aromatic hydrocarbons (PAHs) and hence of soot.[1] The allyl radical is also a key intermediate in tropospheric chemistry. Therefore, its spectral property and chemical behavior have been investigated extensively.

Absorption measurements of the allyl radical have been performed in the visible (vis) and ultraviolet (UV) region.[2−14] The spectral properties of the $\tilde{B}$ and $\tilde{C}$ states have been studied deeply by using resonance-enhanced multiphoton ionization spectroscopy.[10−14] The absorptions in the UV region have been used to obtain reaction rate coefficients associated with the allyl radicals.[5−9] However, relatively little is known about the electronic spectral properties of the transition from the ground ($\tilde{X}$ $^2A_2$) state to the first excited ($\tilde{A}$ $^2B_1$) state. Currie and Ramsay[2] detected the weak absorption in the spectral range of 370−410 nm assigned to the electronic transition between the ground state and first excited state of the allyl radical with a band origin at 408.3 nm during the flash photolysis of various allylic compounds in gas phase. Maier et al.[6] reported the UV/vis absorption spectrum of the allyl radical in an Ar matrix, where an absorption peak in the visible region was 408.5 nm.

The electronically excited states of the allyl radical have been studied by ab initio calculations. Peyerimhoff and Buenker[15] reported the excitation energy of the $\tilde{A}$ $^2B_1 \leftarrow \tilde{X}$ $^2A_2$ transition to be 3.79 eV employing ab initio configuration interaction (CI) calculations based on the molecular orbital method. Ha et al.[16] have also performed an ab initio CI study of the electronic transitions of the allyl radical. The vertical excitation energies and oscillator strengths for several transitions were calculated. Yamaguchi[17] reported the excitation energy of the $\tilde{A}$ $^2B_1 \leftarrow \tilde{X}$ $^2A_2$ transition and vibrational frequencies of the $\tilde{X}$ $^2A_2$ and $\tilde{A}$ $^2B_1$ states at CASSCF level. The adiabatic excitation energy under C_{2v} symmetry was predicted to be 3.04 eV. Oliva et al.[18] calculated the electronic transition energies of the allyl radical by the spin-coupled valence bond theory.

An ultrasensitive direct absorption spectroscopy which is most widely known as cavity ring-down spectroscopy (CRDS) was developed by O'Keefe and Deacon.[19] Yu and Lin[20,21] introduced CRDS detection to the field of chemical kinetics studies. Recently, CRDS has been used to observe absorption spectra of unsaturated hydrocarbon radicals such as vinyl[22−24] and propargyl.[25] In the present work, we report the electronic absorption spectrum of the allyl radical between 370 and 420 nm using CRDS. Ab initio molecular orbital calculations on the adiabatic and vertical excitation energies from the ground state to the first excited state of the allyl radical have been performed to identify the spectral properties of the $\tilde{A} \leftarrow \tilde{X}$ electronic transition. Based on reaction kinetic simulation, the absorption cross sections of the allyl radical in the $\tilde{A} \leftarrow \tilde{X}$ transition have been determined.

2. Experimental Section

The photolysis and cavity ring-down spectroscopy system used for detection of allyl radical has been described in detail previously.[24] A ring-down cavity was 0.625 m long with a pair of high-reflectance mirrors (Los Gatos Research $R > 0.9997$ at 395 nm) with 6 m radius of curvature and 20 mm diameter.

* Corresponding author. E-mail: tonokura@reac.t.u-tokyo.ac.jp.

10.1021/jp001129y CCC: $19.00
Published on Web 08/19/2000

The mirrors covered the wavelength range of 370−430 nm. The reaction cell consisted of a four-way stainless steel cross with the mirrors mounted on stainless steel extension arms, which was evacuated by a mechanical pump with a liquid nitrogen trap. Flexible bellows fixed in the arms allowed adjustment of the mirrors with micrometer screws.

The allyl radicals were produced by an ArF excimer laser (Lambda Physik COMPex 110) photolysis of appropriate gas mixtures. The photolysis laser power used was 1−10 mJ cm^{-2} $pulse^{-1}$. The beam width of the photolysis laser was characterized to be 38 mm by slits. An output of XeCl excimer-pumped dye laser (Lambda Physik LPX 110 + Lambda Physik LPD3002, <10 μJ $pulse^{-1}$) was used as a probe laser beam. The photolysis laser entered the reaction cell at a right angle to the main cell axis and overlapped with the probe laser beam at the center of the cavity. The uniformity of power density of the photolysis laser beam was within 10%. The probe laser beam was spatially filtered through a 50 μm aperture and injected into the cavity through one of the mirrors. The photon intensity decay inside the cavity was monitored by measuring weak transmission of light through the other mirror with a photomultiplier tube (PMT; Hamamatsu R955). A diffuser was placed in front of the PMT to eliminate signal modulations that may arise from inhomogeneities in the spectral sensitivity function of the PMT. The output of the signal from the PMT was fed to a 500 MHz, 1 GS/s digital oscilloscope (Tektronics TDS 520C) and transferred to a Pentium PC via GPIB interface. Typically, ring-down waveforms were averaged over 25 laser shots for each spectral point in the oscilloscope before being transferred to the computer. The intensity decay rate, β, was obtained by fitting the ring-down wave form to a single-exponential decay function, and converted to the absorbance $\langle A \rangle$ via

$$\langle A \rangle = (l/c)(\langle \beta_{abs} \rangle - \langle \beta_{base} \rangle)$$

where l is cavity length and c is the speed of light. $\langle \beta_{abs} \rangle$ is the decay rate in the presence of an absorber, and $\langle \beta_{base} \rangle$ is the base decay rate in the absence of the absorbing species. Absorption spectra were obtained by scanning the wavelength of the probe laser with a spectral resolution of 0.01 nm. For time-dependent studies, timing between the photolysis and probe laser beams was controlled by a pulse generator (Stanford Research Systems DG535). The data acquisition was controlled by LabVIEW virtual instruments (National Instruments, Inc.).

The gases were regulated by calibrated mass flow controllers (KOFLOK 3650). A typical total flow rate was 1500 sccm. To protect the mirrors and the photolysis beam entrance windows from deposition of reaction products, a flow of Ar was introduced over these optical parts. 1,5-Hexadiene and allyl iodide were used as a source of the allyl radical. Ar at 760 Torr (1 Torr ≈ 133.322 Pa) passed through a bubbler containing 1,5-hexadiene (Aldrich 98%) at room temperature (vapor pressure = 200 Torr). On the other hand, allyl iodide (Tokyo Kasei 98%) was freeze−pump−thaw degassed, and then a 5% mixture in the Ar gas was prepared and stored in a glass bulb. The total pressure was measured at the center of the reaction cell with a capacitance manometer (MKS Baratron 622A). Reagent concentrations were calculated from the total pressure and the calibrated flow rates. Typical concentration of the allyl radical formed from photolysis ranged from 10^{12} to 10^{15} molecules cm^{-3}. Spectroscopic and kinetic experiments were carried out at a laser repetition of 1−10 Hz to ensure complete removal of the reacted replenishment of the gas sample between successive laser shots. Experiments were carried out at a total pressure of 20 Torr and at room temperature (297 ± 3 K). The contribution of the diffusion loss (<100 s^{-1}) was negligible under the present experimental conditions.

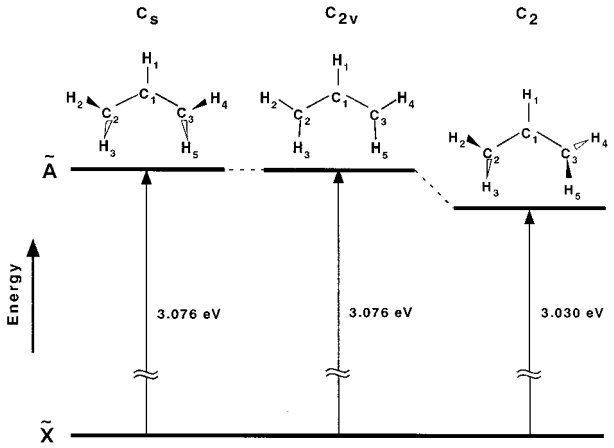

Figure 1. Structures and energetics of the allyl radical (CH_2CHCH_2) in the ground and first excited states.

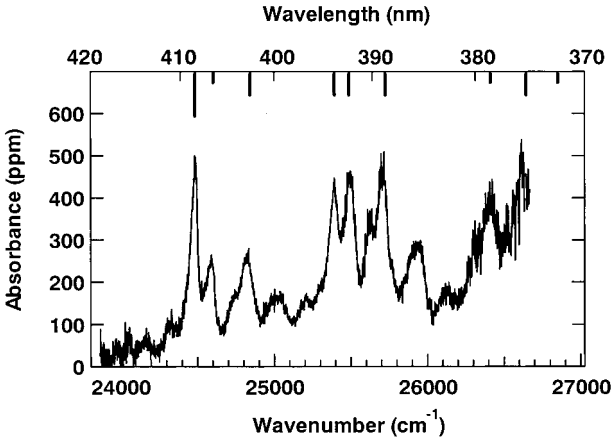

Figure 2. Absorption spectrum of the allyl radical observed from the 193 nm photolysis of 1,5-hexadiene. Delay time between the photolysis and probe laser beams is 10 μs. The stick spectrum shows the positions and relative intensities of allyl radical absorption peaks by Currie and Ramsay.[2]

3. Ab Initio Computational Calculations

The equilibrium geometries of the ground and excited states of the allyl radical were optimized using the complete active space self-consistent field (CASSCF) method. A small active space, including three electrons distributed among three ($1a_2$, $1b_1$, and $2b_1$) orbitals, was used for the calculations of the ground and the first excited states. The DZV(d) and TZV(d,p) basis sets were used. The DZV(d) basis sets are double-ζ basis sets of Huzinaga's (9s5p/4s), which are contracted according to Dunning's [3s2p/2s][26] and augmented with the polarization function of single-ζ d-type added to carbon atom. The TZV-(d,p) basis sets are triple-ζ basis sets of Huzinaga's (10s,6p/5s), which are contracted according to Dunning's [5s3p/3s][27] and augmented with the polarization function of d-type onto carbon atoms and p-type onto hydrogen atoms. Vibrational frequencies of the $\tilde{X}$ and $\tilde{A}$ states were calculated at the CASSCF method. For the ground state, we additionally carried out optimization and vibrational analysis employing the hybrid density functional B3LYP with the 6-311(2+)G* basis set. Adiabatic and vertical excitation energies have been computed by the CASSCF method. The present calculations were carried out using Gaussian 98[28] and GAMESS programs.[29] The

TABLE 1: Optimized Geometries of the Allyl Radical in the Ground and First Excited States[a]

	$\tilde{X}\ ^2A_2$ (C_{2v})				$\tilde{A}\ ^2B_1$ (C_{2v})		$\tilde{A}\ ^2B$ (C_2)	
	CASSCF[b,c] DZV(d)	CASSCF[c] TZV(d,p)	B3LYP[c] 6-311(2+)G*	expt[d]	CASSCF[b,c] DZV(d)	CASSCF[c] TZV(d,p)	CASSCF[e] DZV(d)	CASSCF[e] TZV(d,p)
bond lengths								
$r(C_1C_2)$	1.397	1.386	1.388	1.386	1.473	1.466	1.468	1.459
$r(C_1H_1)$	1.077	1.079	1.091		1.075	1.072	1.077	1.075
$r(C_2H_2)$	1.072	1.075	1.085		1.073	1.073	1.079	1.075
$r(C_2H_3)$	1.074	1.077	1.087		1.074	1.071	1.077	1.074
bond angles								
$\theta(C_2C_1C_3)$	124.7	124.5	125.1	123.96	123.3	123.3	121.5	121.5
$\theta(H_2C_2C_1)$	121.2	121.2	121.7		120.4	120.4	119.8	120.1
$\theta(H_3C_2C_1)$	121.2	121.1	121.1		120.8	120.8	119.2	119.6
dihedral angles								
$\phi(C_3C_1C_2H_2)$							128.5	129.9
$\phi(C_3C_1C_2H_3)$							−28.2	−29.7
energies	−116.498 411	−116.523 014			−116.386 773	−116.409 958	−116.388 537	−116.411 677

[a] Bond lengths in angstroms, bond angles in degrees, and energies in hartrees. [b] From ref 17. [c] C_{2v} symmetry. [d] From ref 31. [e] C_2 symmetry.

TABLE 2: Band Positions (cm^{-1}) for the $\tilde{A} \leftarrow \tilde{X}$ Transition of the Allyl Radical

Currie and Ramay[a]	this work[b]	difference	band name
	24 050	−439	a
	24 167	−322	b
	24 336	−153	c
24 485	24 489	0	d
24 605	24 597	108	e
	24 732	243	f
24 844	24 838	349	g
	25 218	729	h
25 393	25 392	903	i
25 490	25 504	1015	j
	25 611	1122	k
25 726	25 719	1230	l
	25 940	1451	m
	26 134	1645	n
	26 312	1823	o
26 413	26 424	1935	p
26 645	26 617	2128	q
26 852		2367[a]	

[a] From ref 2. [b] Absolute uncertainty of bond centers is $\leq \pm 30$ cm^{-1}.

optimized geometries of the ground and first excited states are shown in Figure 1 and Table 1.

4. Results and Discussion

Absorption Spectrum of the Allyl Radical between 370 and 420 nm. Figure 2 shows an absorption spectrum between 370 and 420 nm resulting from the 193 nm photolysis of 1,5-hexadiene at a delay time between photolysis and CRDS detection of 10 μs at a total pressure of 20 Torr. At the long delay time (>1 ms), the spectral bands decayed and finally vanished; thus this absorption is attributed to transient species. The peak positions of the spectrum are listed in Table 2. The absorption spectrum of this band exhibits no fine structure within the probe laser bandwidth ($\Delta\nu = 0.3$ cm^{-1}). The same absorption spectrum was observed during the 193 nm photolysis of allyl iodide. The peak positions in the spectrum agree with the electronic absorption spectrum of the allyl radical reported by Currie and Ramsay,[2] indicating the production and detection of the allyl radical in these systems. The equilibrium geometry for the ground state has C_{2v} symmetric structure, while for the first excited state C_2 geometry is an energy minimum on the potential energy surface (PES), as discussed below. Adiabatic and vertical excitation energies from the ground to the first excited state calculated by the ab initio calculations are listed in Table 3. The ab initio calculations at the CASSCF(3,3)/TZV-(d,p) levels predict the $\tilde{A}\ ^2B_1 \leftarrow \tilde{X}\ ^2A_2$ vertical excitation energy of 3.338 eV (371.4 nm) is quite close to the strong peaks observed around 370 nm. Therefore, the absorption spectrum measured in the spectral range of 370−420 nm is assigned to the $\tilde{A} \leftarrow \tilde{X}$ electronic transition of the allyl radical. The diffuse character of vibronic lines on the absorption band would be attributed to the homogeneous broadening of the band to predissociation[2] or isomerization to cyclopropyl radical.[17,30]

TABLE 3: Vertical and Adiabatic Excitation Energies (eV) for the $\tilde{A} \leftarrow \tilde{X}$ of Allyl Radical[a]

	adiabatic	vertical	ref
CASSCF/DZV(d)	3.037 (408.3)[b]		ref 17
CASSCF/TZV(d,p)	3.076 (403.1)[b]		this work
CASSCF/DZV(d)	2.990 (414.7)[c]	3.296 (376.2)	this work
CASSCF/TZV(d,p)	3.030 (409.2)[c]	3.338 (371.4)	this work
MO-CI		3.79 (335.1)	ref 15
MO-CI		3.13 (396.1)	ref 16
SCVB		3.19 (388.7)	ref 18
expt[d]	(408.3)		this work
expt[d]	(408.3)		ref 2
expt[d]	(408.5)		ref 6

[a] Values in parentheses are wavelengths. [b] C_{2v} symmetry in the $\tilde{A}$ state. [c] C_2 symmetry in the $\tilde{A}$ state. [d] The most intense peak in the red side.

Comparing the experimental results,[31] the optimized geometry for the ground state has shown a better accuracy for the TZV-(d,p) basic sets than for the DZV(d) basic sets. Table 4 shows the calculated vibrational frequencies of 18 normal modes in the $\tilde{X}$ and $\tilde{A}$ states of the allyl radical. The frequencies calculated at the B3LYP/6-311(2+)G* level with scaling[32] are quite close to the experimental values.[31,33−35] To our knowledge, the experimental values of the vibrational frequencies in the $\tilde{A}$ state have never been reported. Yamaguchi[17] calculated the geometries and vibrational frequencies of the allyl radical in the $\tilde{A}$ state within C_{2v} symmetry at the CASSCF(3,3)/DZV(d) level. The frequencies of three out-of-plane vibrations were imaginary. In the present ab initio calculations at the CASSCF(3,3)/TZV-(d,p) level, the C_{2v} structure has one imaginary frequency in the CH_2 asymmetric twisting mode. It is indicated that the C_{2v} structure collapses to the twisted structure upon optimization allowing an out-of-plane distortion. Thus, the geometry optimization and vibrational analysis of the allyl radical in the $\tilde{A}$ state were performed at C_2 and C_s symmetry. At the CASSCF-(3,3)/TZV(d,p) level, a nonplanar C_2 geometry with twisted CH_2 groups in the $\tilde{A}$ state lies 0.046 eV (371 cm^{-1}) lower in energy than the C_{2v} structure and has no imaginary frequency (Table 4). The electronic term is ^2B. On the other hand, the C_s structure

TABLE 4: Vibrational Frequencies (cm^{-1}) of the Ground and First Excited States of the Allyl Radical

		$\tilde{X}\ ^2A_2\ (C_{2v})$					$\tilde{A}\ ^2B_1\ (C_{2v})$			$\tilde{A}\ ^2B\ (C_2)$	
	mode	CASSCF[a] DZV(d)	CASSCF TZV(d,p)	B3LYP[b] 6-311(2+)G*	expt[c]	expt[d]	CASSCF[a,e] DZV(d)	CASSCF[e] TZV(d,p)		CASSCF DZV(d)	CASSCF TZV(d,p)
a_1	ν_1 CH_2 asym str	3446	3474	3109	3107	3114[f,g]	3470	3461	a	3418	3328
	ν_2 CH str	3360	3293	3019	3051		3403	3353		3367	3421
	ν_3 CH_2 sym str	3232	3153	3008	3019		3359	3232		3313	3326
	ν_4 CH_2 sym sci	1637	1621	1467	1463		1608	1595		1593	1586
	ν_5 CH_2 sym rock	1347	1339	1227	1242		1260	1259		1207	1204
	ν_6 C_3 sym str CH_2 rock	1071	1052	999			980	958		972	961
	ν_7 C_3 bend	448	394	388		426(3),[h] 443(8)[i]	390	356		444	481
a_2	ν_8 CH_2 asym wag	700	723	750			196i	185		567	570
	ν_9 CH_2 asym twist	582	587	527		558(15)[h]	136i	168i		170	212
b_1	ν_{10} CH wag	1022	1027	968	983		318	351	b	816	817
	ν_{11} CH_2 sym wag	716	739	776	801	802[j]	167i	71		555	555
	ν_{12} CH_2 asym twist	547	550	509	501	508(12),[h] 522(8)[i]	155	110		435	424
b_2	ν_{13} CH_2 asym str	3442	3293	3109	3107	3111[f,g]	3464	3353		3417	3330
	ν_{14} CH_2 asym str	3349	3163	3013			3368	3234		3313	3327
	ν_{15} CH_2 sym sci	1618	1597	1462	1477		1534	1531		1541	1539
	ν_{16} CH rock	1514	1520	1383	1389		1365	1369		1349	1349
	ν_{17} C_3 asym str CH rock	1184	1165	1163	1184		1789	1764		1763	1739
	ν_{18} CH_2 asym rock	994	996	907	913		971	968		1010	1019

[a] From ref 17. [b] Scaled by 0.9613. [c] In Ar matrix. From ref 33. [d] In gas phase. [e] *i* indicates the imaginary frequency. [f] From ref 34. [g] From ref 35. [h] From ref 11. [i] From ref 14. [j] From ref 31.

is optimized for the $^2B'$ state with one imaginary frequency in the out-of-plane mode. The adiabatic excitation energy of 3.076 eV is almost the same as that of the C_{2v} symmetric structure. Thus, the C_2 structure corresponds to a minimum on the $\tilde{A}$ state PES. Chen et al.[12−14] pointed out geometric distortion to the nonplanar structure and decrease in the CCC bond angle in the $\tilde{B}$ excited state. They identified the distortion that leads to a double-well potential in the $\tilde{B}$ excited state. The nonplanar $\tilde{A}$ state with the twisted CH_2 groups would also have the double-well potential with inversion doubling of levels at or below the top of barrier. In the present ab initio calculations, the barrier height for the inversion is ca. 400 cm^{-1}, and it is expected that the inversion splittings are large for three modes of ν_7 (481 cm^{-1}), ν_9 (212 cm^{-1}), and ν_{12} (424 cm^{-1}).

According to the electronic selection rule, the transition from $^2A_2$ to $^2B_1$ is allowed. The transition moment lies in the plane of the molecule parallel (*yz*) to the long axis (*y*). The configuration state function of the ground state in C_{2v} geometry is described with the configuration $(core)(1b_1)^2(1a_2)^1(2b_1)^0$, where $1b_1$, $1a_2$, and $2b_1$ are bonding, nonbonding, and antibonding orbitals, respectively. The first excited state can be mainly described by two molecular orbital configurations, $(core)(1b_1)^1(1a_2)^2(2b_1)^0$ and $(core)(1b_1)^2(1a_2)^0(2b_1)^1$. They are obtained by promoting one electron from $1b_1$ to $1a_2$ or by replacing $1a_2$ by $2b_1$. The $\tilde{A} \leftarrow \tilde{X}$ transition is characterized to valence excitation. The occupation numbers of three natural orbitals in the $\tilde{A}$ state are 1.33, 1.14, and 0.53. At C_2 symmetry, the molecular orbitals change to 5b, 7a, and 6b with the occupation numbers of 1.20, 1.31, and 0.49, respectively.

The CCC bond angle decreases from 124.5° for the $\tilde{X}$ state with C_{2v} geometry to 121.5° in the $\tilde{A}$ state with C_2 symmetry, as shown in Table 1. A CC bond lengthens from 1.39 Å for the $\tilde{X}$ state to 1.46 Å for the $\tilde{A}$ state. The elongation of the CC bond is due to the reduction of the C−C π-bonding population in the $\tilde{A}$ state. In the $\tilde{A}$ state, vibrational frequencies change substantially. All out-of-plane a_2 and b_1 normal modes decrease their frequencies in the $\tilde{A}$ state. For instance, the ν_9 frequency of the CH_2 twist vibration decreases from 587 to 212 cm^{-1}. The frequency change is caused by the out-of-plane distortion in the $\tilde{A}$ state. The Q_6 normal mode, responsible for the coupling between C_3 symmetric stretching and CH_2 rocking, decreases from 1052 to 961 cm^{-1}. The Q_{17} normal mode, corresponding to C_3 asymmetric stretching coupled with CH rocking, exhibits an increase in its frequency from 1165 to 1739 cm^{-1}. This is due to the elongation of the CC bond in the $\tilde{A}$ state.

The present calculations at the CASSCF(3,3)/TZV(d,p) level predicts the adiabatic excitation energies to the C_2 symmetric structure of 3.030 eV (409.2 nm). This value is in quantitative agreement with the absorption peak at 408.3 nm. Several new peaks were observed in the red side of this peak. These new peaks confirmed from both 1,5-hexadiene and allyl iodide precursors are assigned to hot bands. A frequency shift of −439 cm^{-1} at band a is consistent with the ν_7 C_3 bending frequency in the $\tilde{X}$ state. Since the CC bond is lengthened in the $\tilde{A}$ state, the CC stretching mode would be prominent in the absorption spectrum. The CH_2 twisting mode would also be significant in the spectrum because of the out-of-plane distortion in the $\tilde{A}$ state. Fundamental frequencies of 243, 903, and 1230 cm^{-1} are derived from the absorption spectrum. These values are compared with the values obtained in the ab initio calculations of 212, 961, and 1204 cm^{-1} assigned to CH_2 asymmetric twisting, C_3 symmetric stretching coupled with CH_2 rocking, and CH_2 symmetric rocking, respectively. There are several unassignable bands, e.g., bands e (108 cm^{-1}) and g (349 cm^{-1}), in the absorption spectrum. It is expected that the double well potential problem would induce complication on the spectral structure. The vibronic bands would be assigned by the measurements under a supersonic expansion condition and of the spectra of isotopic species.

Absorption Cross Sections of the Allyl Radical. The end product analysis of the 193 nm photolysis of 1,5-hexadiene by Tulloch et al.[5] deduced the following photodissociation processes:

$$CH_2{=}CHCH_2CH_2CH{=}CH_2 + 193\ nm \rightarrow 2CH_2CHCH_2 \quad (1)$$

$$\rightarrow CH_2{=}CHCH_3 + CH_2{=}C{=}CH_2 \quad (2)$$

$$\rightarrow CH_2{=}CHCH{=}CH_2 + CH_2{=}CH_2 \quad (3)$$

$$\rightarrow C_5H_7 + CH_3 \quad (4)$$

The relative yield of the photolysis channels was established

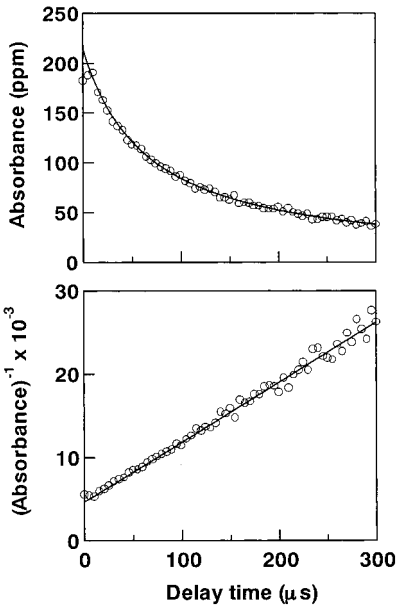

Figure 3. Time traces of the allyl radical produced from the 193 nm photolysis of 1,5-hexadiene. (a) Absorbance at 402.9 nm with delay time between photolysis and probe laser. (b) Time trace of a reciprocal of absorbance versus delay time. A solid line is a least-squares fit to the experimental data.

as 68:27:2.5:2.5.[5] Thus CH_2CHCH_2 represents 96% of the radical products. They reported that CH_2CHCH_2 would not react with any of the molecular products and parent molecule; therefore the reaction of C_5H_7 with allyl to form C_8H_{12} was not detected.[5] Contribution of the reaction associated with C_5H_7 and CH_3 radicals is small (<4%) because of the low quantum yield of C_5H_7 and CH_3. Thus, the time dependence of allyl radical concentration would be governed predominantly by the CH_2-$CHCH_2-CH_2CHCH_2$ reaction.[5]

$$2CH_2CHCH_2 + M \rightarrow CH_2{=}CHCH_2CH_2CH{=}CH_2 + M \quad (5)$$

This recombination reaction is at the high-pressure limit over the range of 1−250 Torr.[5] When the laser line width is much narrower compared with the width of the absorption feature of interest, the absorption measurements in CRDS provide accurate measurements of the number densities.[19] Since the absorption spectrum of the allyl radical exhibits diffuse character, accurate measurements of allyl radical concentration should be provided in the present experiments. Figure 3 shows a typical time profile of the allyl radical produced from the 193 nm photolysis of 1,5-hexadiene at 402.9 nm. The points represent the absorbance of the allyl radical as a function of delay time. A plot of a reciprocal of absorbance versus delay time at 402.9 nm is linear (Figure 3b), indicating that the allyl was displaying second-order kinetic behavior associated with the self-reaction of allyl radical. Second-order kinetic behaviors were observed at all wavelengths investigated. The decay traces were analyzed by a nonlinear least-squares fitting procedure to allow determination of k_5/σ at the monitoring wavelength. The mean value of k_5/σ obtained at 402.9 nm is $(1.4 \pm 0.1) \times 10^8$ cm s^{-1}. The rate constant for recombination of the allyl radicals at the room temperature was determined by the measurements of k_5/σ around 220 nm.[4,5,9] Van den Bergh and Callear[4] obtained a value of $(1.41 \pm 0.6) \times 10^{-11}$ cm^3 molecule^{-1} s^{-1} using the flash lamp photolysis of 1,5-hexadiene over the wavelength range of 185−205 nm. Tulloch et al.[5] obtained a value of $(2.65 \pm 0.20) \times 10^{-11}$ cm^3 molecule^{-1} s^{-1} at 295 K. Jenkin et al.[9] reported a value of $(3.0 \pm 0.5) \times 10^{-11}$ cm^3 molecule^{-1} s^{-1} at 296 K. Tulloch et al. and Jenkin et al. used the 193 nm laser photolysis of 1,5-hexadiene as a source of allyl. Van den Bergh and Callear reported a small contribution at 216 nm due to the presence of CH_3 in the initial radical concentration, which also implies the existence of one or more isomeric C_5H_7 radicals, formed simultaneously from reaction 4. If a significantly greater relative concentration of these radicals was generated by broad-band photolysis, some complication in the determination of k_5/σ might result. Using the average value of k_5 determined in the 193 nm laser photolysis experiments and the value of k_5/σ obtained in the present study gives $\sigma = (2.0 \pm 0.4) \times 10^{-19}$ cm^2 molecule^{-1} at 402.9 nm. The error limits indicate one standard deviation and include uncertainties in k_5 and k_5/σ and uniformity for the beam pattern of the photolysis laser.

Oth et al.[36] reported that the oscillator strength (f_{osc}) associated with the $\tilde{A}\ ^2B_1 \leftarrow \tilde{X}\ ^2A_2$ transition (0.0013) was more than 2 orders of magnitude lower than that in the spectral range of 200−240 nm (0.234) in an Ar matrix. In the gas phase, the value of the oscillator strength ($f_{osc} = 0.26$) in this region reported by Nakajima and Yoshihara[8] corresponds to that obtained in the Ar matrix. The absorption cross section maximum ($\lambda = 222.5$ nm) of this band was established to be 6.14×10^{-17} cm^2 molecule^{-1}.[9] From these values the absorption cross section of the $\tilde{A}\ ^2B_1 \leftarrow \tilde{X}\ ^2A_2$ transition is estimated roughly to be $\sim 10^{-19}$ cm^2 molecule^{-1}. The absorption cross section obtained in the present study is in reasonable agreement with this value.

We have confirmed that the photolysis laser power dependence on the initial concentration of the allyl radical was first order in the range of 1−10 mJ cm^{-2} pulse^{-1}. The absorption cross section of the allyl radical can be calculated directly from absorbance, initial concentration of the allyl radical, $[C_3H_5]_0$, and absorption path length, l_s:

$$\langle A \rangle = \sigma_{C_3H_5}[C_3H_5]_0 l_s \quad (6)$$

Based on the photoabsorption cross section of $\sigma_{193} = (4.1 \pm 0.5) \times 10^{-18}$ cm^2 molecule^{-1} for 1,5-hexadiene[37] and the photon density we used, the fraction of light absorbed by 1,5-hexadiene (f_{abs}) is calculated. A dissociation quantum yield (ϕ_{diss}) of 0.9 for the 193 nm photolysis of 1,5-hexadiene is deduced from the results of Shimo et al.[7] This value combined with f_{abs} yields the initial concentration of the allyl radical. Absorbances are measured, leading to a value of $(2 \pm 1) \times 10^{-19}$ cm^2 molecule^{-1} for the absorption cross sections of the allyl radical at 402.9 nm.

5. Conclusions

We have measured the absorption spectrum assigned to the $\tilde{A} \leftarrow \tilde{X}$ transition of the allyl radical in the range of 370−420 nm by cavity ring-down spectroscopy. The diffuse character on the vibronic bands attributed to predissociation or to isomerization was observed. The nonplanar C_2 structure with CH_2 twisted group was found to be a potential minimum in the $\tilde{A}$ state by the ab initio molecular orbital calculations at CASSCF levels. Vibrational frequencies of all a_2 and b_1 normal modes decrease in the $\tilde{A}\ ^2B$ state because of out-of-plane distortion. The CC stretching and CH_2 twisting modes are expected to be predominant in the absorption spectrum. Based on the reaction kinetic simulation associated with the self-reaction of the allyl radical, the absorption cross section of the allyl radical was estimated to be $\sigma = (2.0 \pm 0.4) \times 10^{-19}$ cm^2 molecule^{-1} at 402.9 nm.

Acknowledgment. This work was supported in part by a grant-in-aid from the Ministry of Education, Science, Sports and Culture (No. 10640483) and the Sumitomo Foundation.

References and Notes

(1) Westmorel, P. R.; Dean, A. M.; Howard, J. B.; Longwell, J. P. *J. Phys. Chem.* **1989**, *93*, 817.
(2) Currie, C. L.; Ramsay, D. A. *J. Chem. Phys.* **1966**, *45*, 488.
(3) Callear, A. B.; Lee, H. K. *Trans. Faraday Soc.* **1968**, *64*, 308.
(4) Van den Bergh, H. E.; Callear, A. B. *Trans. Faraday Soc.* **1970**, *66*, 2681.
(5) Tulloch, J. M.; Macpherson, M. T.; Morgan, C. A.; Pilling, M. J. *J. Phys. Chem.* **1982**, *86*, 3812.
(6) Maier, G.; Reisenauer, H. P.; Rohde, B.; Dehnicke, K. *Chem. Ber.* **1983**, *116*, 732.
(7) Shimo, N.; Nakashima, N.; Ikeda, N.; Yoshihara, K. *J. Photochem.* **1986**, *33*, 279.
(8) Nakashima, N.; Yoshihara, K. *Laser Chem.* **1987**, *7*, 177.
(9) Jenkin, M. E.; Murrells, T. P.; Shalliker, S. J.; Hayman, G. D. *J. Chem. Soc., Faraday Trans.* **1993**, *89*, 433.
(10) Hudgens, J. W.; Dulcey, C. S. *J. Phys. Chem.* **1985**, *89*, 1505.
(11) Sappey, A. D.; Weisshaar, J. C. *J. Phys. Chem.* **1987**, *91*, 3731.
(12) Minsek, D. W.; Blush, J. A.; Chen. P. *J. Phys. Chem.* **1992**, *96*, 2025.
(13) Blush, J. A.; Minsek, D. W.; Chen. P. *J. Phys. Chem.* **1992**, *96*, 10150.
(14) Minsek, D. W.; Chen. P. *J. Phys. Chem.* **1993**, *97*, 13375.
(15) Peyerimhoff, S. D.; Buenker, R. J. *J. Chem. Phys.* **1969**, *51*, 2528.
(16) Ha, T.; Baumann, H.; Oth, J. F. M. *J. Chem. Phys.* **1986**, *85*, 1438.
(17) Yamaguchi, M. *J. Mol. Struct. (THEOCHEM)* **1996**, *365*, 143.
(18) Oliva, J. M.; Gerratt, J.; Copper, D. L.; Karadakov, P. B.; Raimondi, M. *J. Chem. Phys.* **1997**, *106*, 3663.
(19) O'Keefe, A.; Deacon, D. A. G. *Rev. Sci. Instrum.* **1988**, *59*, 2544.
(20) Yu, T.; Lin, M. C. *J. Am. Chem. Soc.* **1993**, *115*, 4371.
(21) Yu, T.; Lin, M. C. *Int. J. Chem. Kinet.* **1993**, *25*, 875.
(22) Pibel, C. D.; Mclloy, A.; Taatjes, C. A.; Alfred, S.; Patrick, K.; Halpern, J. B. *J. Chem. Phys.* **1999**, *110*, 1841.
(23) Fahr, A.; Hassanzadeh, P.; Atkinson, D. B. *Chem. Phys.* **1998**, *236*, 43.
(24) Tonokura, K.; Marui, S.; Koshi, M. *Chem. Phys. Lett.* **1999**, *313*, 771.
(25) Atkinson, D. B.; Hudgens, J. W. *J. Phys. Chem. A* **1999**, *103*, 4242.
(26) Dunning, T. H.; Hay, O. J. *Modern Theoretical Chemistry*; Shafer III, H. F., Ed.; Plenum: New York, 1977; Vol. 3, pp 1−27.
(27) Dunning, T. H. *J. Chem. Phys.* **1971**, 55, 716.
(28) Frisch, M. J.; Trucks, G. W.; Schlegel, H. B.; Scuseria, G. E.; Robb, M. A.; Cheeseman, J. R.; Zakrzewski, V. Z.; Montgomery, Jr., J. A.; Stratmann, R. E.; Burant, J. C.; Dapprich, S.; Millam, J. M.; Daniels, A. D.; Kudin, K. N.; Strain, M. C.; Farkas, O.; Tomasi, J.; Barone, V.; Cossi, M.; Cammi, R.; Mennucci, B.; Pomelli, C.; Adamo, C.; Clifford, S.; Ochterski, J.; Petersson, G. A.; Ayala, P. Y.; Cui, Q.; Morokuma, K.; Malick, D. K.; Rabuck, A. D.; Raghavachari, K.; Foresman, J. B.; Cioslowski, J.; Ortiz, J. V.; Baboul, A. G.; Stefanov, B. B.; Liu, G.; Liashenko, A.; Piskorz, P.; Komaromi, I.; Gomperts, R.; Martin, R. L.; Fox, D. J.; Keith, T.; Al-Laham, M. A.; Peng, C. Y.; Nanayakkara, A.; Gonzalez, C.; Challacombe, M.; Gill, P. M. W.; Johnson, B.; Chen, W.; Wong, M. W.; Andres, J. L.; Gonzalez, C.; Head-Gordon, M.; Replogle, E. S.; Pople, J. A. *Gaussian 98*, Revision A.7; Gaussian, Inc.: Pittsburgh, PA, 1998.
(29) Schmidt, M. W.; Baldridge, K. K.; Boatz, J. A.; Elbert, S. T.; Gordon, M. S.; Jensen, J. H.; Koseki, S.; Matsunaga, N.; Nguyen, K. A.; Su, S. J.; Windus, T. L.; Dupuis, M.; Montgomery, J. A. *J. Comput. Chem.* **1993**, *14*, 1347.
(30) Holtzhauer, K.; Cometta-Morini, C.; Oth, J. F. M. *J. Phys. Org. Chem.* **1990**, *3*, 219.
(31) Hirota, E.; Yamada, C.; Okunishi, M. *J. Chem. Phys.* **1992**, *97*, 2963.
(32) The ratio of calculated frequencies scaled by 0.9613 to experimental frequencies in the Ar matrix was 0.993 ± 0.01 (1σ).
(33) Mal'tsev, A. K.; Korolev, V. A.; Nefedov, O. M. *Bull. Acad. Sci. USSR, Div. Chem. Sci.* **1984**, *33*, 510.
(34) Uy, D.; Davis, S.; Nesbit, D. J. *J. Chem. Phys.* **1998**, *109*, 7793.
(35) DeSain, J. D.; Thompson, R. I.; Sharma, S. D.; Curl, R. F. *J. Chem. Phys.* **1998**, *109*, 7803.
(36) Oth, J. F. M.; et al. Unpublished results.
(37) The absorption cross section was determined in the present study.